Cite as:
M. Česnik, J. Slavič and M. Boltežar,
Uninterrupted and accelerated vibrational fatigue testing with simultaneous monitoring of the natural frequency and damping,
Journal of Sound and Vibration, Vol. 331(2012), 5370–5382,
DOI: 10.1016/j.jsv.2012.06.022

Uninterrupted and accelerated vibrational fatigue testing with simultaneous monitoring of the natural frequency and damping

Martin Česnik[a], Janko Slavič[a], Miha Boltežar[a,*]

[a] *University of Ljubljana, Faculty of Mechanical Engineering, Aškerčeva 6, 1000 Ljubljana, SI, Slovenia*

Abstract

A mechanical system's modal parameters change when fatigue loading is applied to the system. In order to perform an accelerated vibration-based fatigue test these changes must be taken into account in order to maintain constant-stress loading. This paper presents an improved accelerated fatigue-testing methodology based on the dynamic response of the test specimen to the harmonic excitation in the near-resonant area with simultaneous monitoring of the modal parameters. The measurements of the phase angle and the stress amplitude in the fatigue zone are used for the real-time adjustment of the excitation signal according to the changes in the specimen's modal parameters. The presented methodology ensures a constant load level throughout the fatigue process until the final failure occurs. With the proposed testing methodology it is possible to obtain a S-N point of the Woehler curve relatively quickly and to simultaneously monitor the changes

*Corresponding author. Tel.: +386 14771 608.
Email address: miha.boltezar@fs.uni-lj.si

of the specimen's natural frequency and damping loss factor. The presented methodology with real-time control is verified on an aluminium Y-shaped specimen (10^6 load cycles are achieved in 21 minutes) and is applicable to a specimen with arbitrary geometry. Besides the faster completion of the fatigue test the methodology can be adopted for the validation of the vibrational fatigue analysis.

Keywords: Accelerated fatigue testing, Vibrational fatigue, Failure prediction, Experimental setup

---

1. Introduction

The changes to the modal parameters of a structure when subjected to a fatigue load are widely known and used in various fields. In the past two decades much research has been done in the area of global vibration-based damage detection [1, 2, 3], which recognizes the time and location of the fatigue failure by monitoring the changes to the modal parameters of the structure (natural frequencies, damping loss factors and mode shapes). Besides damage detection the change of the modal parameters can also be utilized for a *fatigue failure prediction* during the service life of the structure.

An extensive review of the methods for damage prediction based on changes to the modal parameters was made by Doebling *et al.* [4]. An application of failure prediction based on modal parameters was reported by Bedewi and Kung [5], who predicted the residual life of composite structures by monitoring the decreasing trend in natural frequency and the increasing trend in damping loss factor as a function of the load cycles during a fatigue test. Similar observations of the modal parameters were made by Shang *et al.* [6] for spot-welded joints, for which an empirical fatigue-damage model based on the natural frequency change was researched by Wang *et al.* [7]. In order to illustrate the feasibility of the modal approach for failure prediction at a more fundamental level Giannoccaro *et al.* [8] measured changes in the resonance and anti-resonance of notched steel specimens when subjected to a tensile fatigue load. Similarly, for a simple aluminium alloy beam Colakoglu and Jerina [9] observed an increase in the damping loss factors during the fatigue process, which was also used as a damage-detection method for the health monitoring of a reinforced concrete frame [10].

In most of the aforementioned investigations [6, 7, 10, 11] the authors performed a standard fatigue test of the specimen [12, 13] using servo-hydraulic testing machine, which was stopped after a certain number of cycles and the frequency-response function was obtained by using impulsive excitation with an impact hammer. Vanlanduit *et al.* [14] performed an uninterrupted fatigue test with simultaneous natural-frequency tracking. In their research the excitation, applied with an electro-dynamical shaker, was composed of two multi-sine signals: a low-frequency fatigue load and a high-frequency dynamic load. The failure of the tested steel beam occurred in the low-frequency fatigue area after 2000 cycles. In the field of civil engineering the continuous, near-real-time tracking of the modal properties of a structure [15] was shown to be useful for the rapid evaluation of the health conditions of a structure during and after a seismic event.

Resonant fatigue-testing machines (*i.e.* Amsler Vibrophore, Rumul Vibroforte) were used by Audenino *et al.* [16, 17] in their research of non-linear internal damping in metals and its correlation to thermography. These machines excite the specimen with additional weights in the resonant area by applying the excitation force to the weights and can work in the frequency area up to 300 Hz.

A further development of the fatigue testing in the resonant area was made by George *et al.* [18], who developed a new methodology based on the dynamic response of the kinematically excited test specimen in the near-resonant area. The proposed methodology can be performed with an electro-dynamical shaker, to which the specimen needs to be fastened. The results for a high-cycle fatigue stress of the titanium alloy Ti-6Al-4V obtained with a vibration-based methodology are in accordance with the results obtained with classical fatigue testing [19]. This vibration-based fatigue testing was later enhanced [20] to perform fatigue tests with different mean stresses and stress ratios. George *et al.* noticed a change in the specimen's natural frequency during the fatigue testing and therefore manually adjusted the excitation frequency to keep the deviation of the actual load stress from the desired load stress to within 5%.

In recent years the scope of accelerated vibration-based fatigue testing has broadened as researchers have applied different types of excitation to the test specimens. French *et al.* [21] performed durability testing of notched beams by exciting the specimens in three directions with sine sweeps in the area of the specimens' resonance. Furthermore, the excitation for a accelerated vibrational fatigue test can be performed by means of the electromagnetic forces in an alternating magnetic field, as demonstrated by Kheng [22] in a fatigue test of a cantilever spring mechanism.

This research improves on the approach of George *et al.* [18] by testing at near resonance with a real-time phase-locked control loop, which improves the control of the stress load level. With this enhancement it is possible to monitor the instantaneous modal parameters without any interruptions to the fatigue test. The methodology presented in paper can be conveniently used in the vibration fatigue analysis of dynamic structures exposed to vibration excitation [23, 24]. The present paper is organized as follows. In Section 2 the theoretical background and structural dynamics of the proposed Y-shaped specimen are studied. In Section 3 the experimental setup with the corresponding shaker-control software is presented. In Section 4 the experimental results are analyzed to prove the feasibility of the proposed method.

2. Theoretical background

When a dynamic system is excited in the resonant area a response amplification can be observed. By taking advantage of this response amplification it is possible to achieve high stresses in the specimen by applying relatively small excitation forces, which makes an electro-dynamic shaker suitable for performing fatigue tests. The idea of the accelerated vibrational fatigue test is based on the dynamic response of the specimen; therefore, it is necessary to research the dynamic properties of the specimen before the actual fatigue test.

2.1. Specimen's dynamic response

The dynamic response of the specimen depends on the modal properties of the specimen; *i.e.*, natural frequencies, mode shapes and damping loss factors. The natural frequencies and mode shapes are easily obtained using the finite-element method. The damping loss factor of the particular mode shape can only be determined experimentally; however, in the case of lightly damped structures the value of the damping loss factors do not noticeably change the positions of the natural frequencies [25]. For an in-resonance fatigue test the modal properties must comply with three main guidelines [18]:

1. the specimen's natural frequency of interest must be well separated from the remaining natural frequencies and be within the shaker's frequency range,

2. the specimen's mode shape of interest must be excitable with a translational movement in the axis of the shaker,
3. the fatigue zone, where the maximum stresses in the specimen occur, must be located on a surface that is appropriate for strain-gauge measurements.

Regardless of the specimen geometry, the numerical modal analysis should always be performed to confirm that the proposed geometry complies with the stated guidelines. In the case of the biaxial fatigue zone stress state the ratio of the monitored principal stress σ_1 to the equivalent stress σ_{eq} [26] must also be determined.

In this research the Y-shaped specimen shown in Fig. 1(a) is used. The main three beams are arranged at 120° around the main axis and have a rectangular cross-section of 10×10 mm. The Y-shaped specimen was made from aluminium alloy A-S8U3 [27, 28] by casting and with a surface finish performed by milling. The fatigue zone was additionally fine-ground in order to remove any scratches that could cause the premature start of an initial crack. Two additional features are included in the Y-shaped design: steel dead-weights of 52.5 g and a round hole through the main axis, which are used to adjust the initial natural frequency and to position the fatigue zone on a suitable surface, respectively.

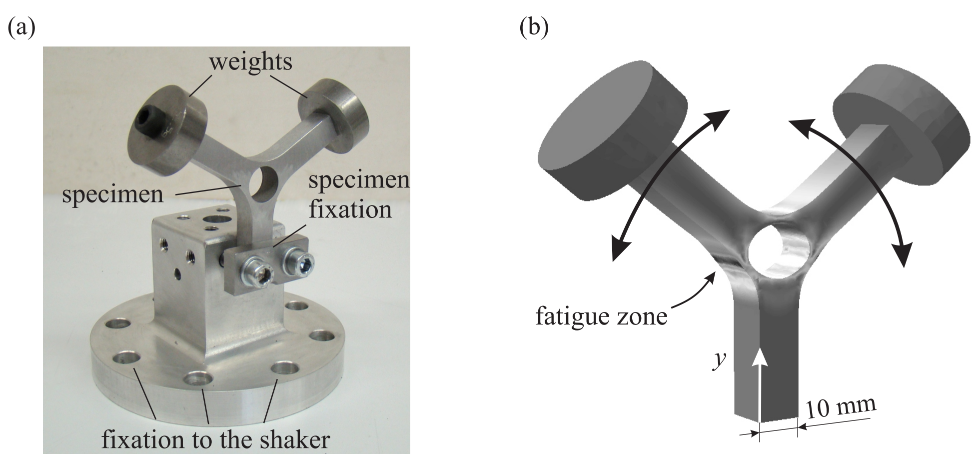

Figure 1: (a) Fixed specimen, (b) specimen's fourth-mode shape - σ_{eq}.

By evaluating the dynamic response of the Y-shaped specimen according to the stated guidelines, the fourth-mode shape at $\omega_1 = 794$ Hz[1] (Fig. 1(b)) was recognized as the most suitable for the near-resonance fatigue test.

The stress state in the fatigue zone, marked in Fig. 1(b), is biaxial. The ratio of the equivalent to the principal stress is $\sigma_{\mathrm{eq}}/\sigma_1 = 0.902$, which must be taken into account when constructing the Woehler curve, since σ_{eq} represents the proper fatigue criterion for biaxial stress states [29].

2.2. Stress measurement during the changes of the modal properties

During the accelerated fatigue test the changes to the modal parameters of the specimen occur [6, 9], which consequently alter the specimen's response. In order to maintain a constant stress during the accelerated fatigue test it is necessary to design a special control methodology, which is explained in detail in Section 3. However, the constant stress control, further explained in Section 3.2, requires some preliminary theoretical analysis, which follows.

The basic outline of the accelerated vibration fatigue experiment is illustrated in Fig. 2. The base of the Y-shaped specimen is excited with a ground motion of:

$$y(t) = Y\,\mathrm{e}^{\mathrm{i}\omega t}, \tag{1}$$

where Y denotes the excitation amplitude and ω the excitation frequency. The specimen's response to harmonic excitation can be defined by the total response displacement $x_1^{\mathrm{T}}(t)$ (see Fig. 2) as:

$$x_1^{\mathrm{T}}(t) = \overline{X}_1^{\mathrm{T}}\,\mathrm{e}^{\mathrm{i}\omega t}, \tag{2}$$

where $\overline{X}_1^{\mathrm{T}} = X_1^{\mathrm{T}}\,\mathrm{e}^{\mathrm{i}\phi}$ is a phasor, X_1^{T} denotes the total response displacement amplitude and ϕ is the phase angle.

Traditionally, the principal stress σ_1 is measured with a strain gauge. However, while performing the accelerated fatigue test we found that the strain gauge suffered fatigue failure before the failure of the specimen. Furthermore, the installation of the strain sensor is very sensitive to the position on the specimen and is also very time consuming. Consequently, an alternative, indirect method for the stress measurement is proposed in this research.

[1]For the sake of simplicity the fourth natural frequency is denoted as ω_1 rather than ω_4.

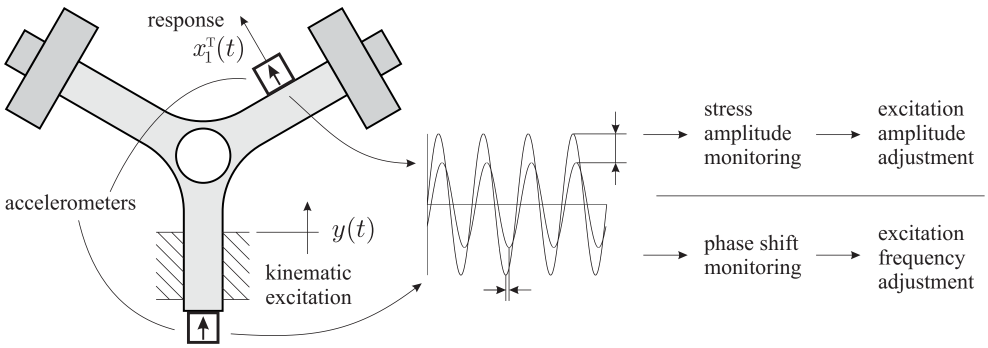

Figure 2: Experimental setup outline.

The proposed indirect stress-measurement method is based on the fundamentals of a modal analysis, described in the following deduction. Continuous structures, such as a Y-shaped specimen, are generally described as MDOF systems (Fig. 3); in the case of a kinematic excitation and a hysteretic damping mechanism the equilibrium equation can be written as [30]:

$$\mathbf{M}\,\ddot{\mathbf{x}}^{\mathrm{T}} + \mathrm{i}\,\mathbf{D}\,\mathbf{x}^{\mathrm{T}} + \mathbf{K}\,\mathbf{x}^{\mathrm{T}} = \mathbf{0}. \tag{3}$$

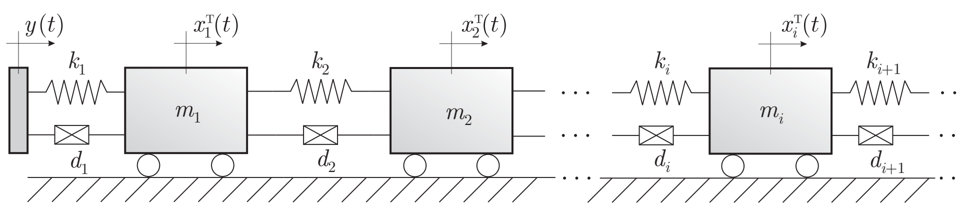

Figure 3: Representation of a MDOF system with a kinematic excitation.

Here $\mathbf{x}^{\mathrm{T}}$ denotes the total displacement vector and $\mathbf{M}$, $\mathbf{D}$ and $\mathbf{K}$ are the mass, damping and stiffness matrices, respectively. For a general case $\mathbf{x}^{\mathrm{T}}$ is [31]:

$$\mathbf{x}^{\mathrm{T}}(t) = \mathbf{x}(t) + \boldsymbol{\iota}\,y(t), \tag{4}$$

where $\mathbf{x}(t)$ is a vector of relative response displacements and $\boldsymbol{\iota}$ is the direction influence vector. According to the Eqs. (3) and (4) the the system's relative response $\overline{X}_a$ of the a-th degree-of-freedom in the case of the base excitation $y(t)$ is deduced as [30]:

$$\overline{X}_a = \mathbf{m}_a\,\boldsymbol{\iota}\,\omega^2\,Y\,\alpha_{X\,a}(\omega) = \mathbf{m}_a\,\boldsymbol{\iota}\,\omega^2\,Y\,\sum_{r=1}^{N}\frac{{}_rA_{X\,a}}{\omega_r^2 - \omega^2 + \mathrm{i}\,\eta_r\omega_r^2}, \tag{5}$$

where $\mathbf{m}_a$ denotes the a-th row in the mass matrix $\mathbf{M}$ and $\alpha_{X\,a}(\omega)$ the receptance function for the a-th degree of freedom. Additionally, ${}_rA_{X\,a}$ represents the mass-normalized modal constant for the a-th degree-of-freedom, ω_r is the r-th natural frequency and η_r is the hysteretic damping loss factor for the r-th mode shape. Here it should be noted that since the excitation and response are single harmonics with a known frequency ω the relations $\ddot{x}(t) = -\omega^2 \cdot x(t)$ and $\ddot{y}(t) = -\omega^2 \cdot y(t)$ between the measured accelerations and displacements are valid.

If a dynamic system is observed when excited near the p-th natural frequency the the ratio $\overline{X}_a/Y$ can be approximated as [30]:

$$\frac{\overline{X}_a}{Y} \approx \mathbf{m}_a\, \boldsymbol{\iota}\, \omega^2 \left(\frac{{}_pA_{X\,a}}{\omega_p^2 - \omega^2 + \mathrm{i}\eta_p\omega_p^2} + B_{X\,a} \right), \tag{6}$$

where $B_{X\,a}$ is a constant complex quantity, in which the contribution of the remaining modes $r \neq p$ is accounted for.

If the Y-shaped specimen is observed, a similar deduction to that in Eq. (6) can be made for the frequency response of the measured principal stress $\overline{\sigma}_1$ to the base excitation $y(t)$ as:

$$\frac{\overline{\sigma}_1}{Y} = \mathbf{m}_{\sigma_1}\, \boldsymbol{\iota}\, \omega^2\, \alpha_{\sigma_1}(\omega) = \mathbf{m}_{\sigma_1}\, \boldsymbol{\iota}\, \omega^2 \left(\frac{{}_pA_{\sigma_1}}{\omega_p^2 - \omega^2 + \mathrm{i}\eta_p\omega_p^2} + B_{\sigma_1} \right), \tag{7}$$

where the mass-normalized modal constant and the contribution of the remaining modes are denoted as ${}_pA_{\sigma_1}$ and B_{σ_1}, respectively. $\mathbf{m}_{\sigma_1}$ is a vector of constant values, related to the mass matrix.

In the case of the Y-shaped specimen the total response is denoted as $x_1^{\mathrm{T}}(t)$ (Fig. 2); therefore, the relative displacement amplitude X_1 between excitation amplitude $y(t)$ and the response $\overline{X}_1^{\mathrm{T}}$ is written as (Eqs. (1, 2)):

$$X_1 = \left| \overline{X}_1^{\mathrm{T}} - Y \right|. \tag{8}$$

Introducing the transmissibilities from Eqs. (6) and (7) it follows:

$$\frac{\sigma_1}{X_1}(\omega_p, \eta_p) = \frac{\left| \frac{{}_pA'_{\sigma_1}}{\omega_p^2 - \omega^2 + \mathrm{i}\eta_p\omega_p^2} + B'_{\sigma_1} \right|}{\left| \frac{{}_pA'_{X_1}}{\omega_p^2 - \omega^2 + \mathrm{i}\eta_p\omega_p^2} + B'_{X_1} \right|}, \tag{9}$$

where $'$ denotes the multiplication of the modal constant ${}_pA$ by the corresponding mass-related matrix of constants $\mathbf{m}_{\sigma_1}$.

In order to investigate the actual value of the σ_1/X_1 ratio for the Y-shaped specimen and its changes during the accelerated fatigue test, a theoretical dynamic system is introduced. This dynamic system must represent the actual dynamic response of a Y-shaped specimen during an accelerated fatigue test; therefore, two assumptions must be made. Firstly, the observed natural frequency ω_1 and the damping loss factor η_1 can change ($\omega_p, \eta_p \neq$ const.) during an accelerated fatigue test before the failure occurs [6, 9]. Secondly, the changes to the modal constants ${}_pA'_{\sigma_1}, B'_{\sigma_1},\ {}_pA'_{X_1}$ and B'_{X_1} have a negligible influence on the system's response before the failure occurs and can be considered as constant compared to the changes of ω_1 and η_1. With the latter assumption it is possible to investigate the frequency response of the σ_1/X_1 ratio during the accelerated fatigue test and to conduct the ω_1 and η_1 identification procedure, as described in Section 2.3.

The dynamic response of the theoretical dynamic system should be similar to the response of the actual Y-shaped specimen, therefore the measured response of the Y-shaped specimen will be adopted for the deduction of the receptance of the theoretical system. The first natural frequency coincides with the measured initial natural frequency, $\omega_1 = 793.3$ Hz, the initial damping loss factor is $\eta_1 = 0.00075$ and the initial dynamic amplifications are $X_1/Y = 24.1$ and $\sigma_1/Y = 97.9$ MPa/μm. The constant frequency difference is $\Delta\omega = \omega - \omega_1 = 3.7$ Hz. To include the influence of the remaining, well-separated modes, an additional natural frequency is introduced at an arbitrary frequency value; in the present analysis $\omega_2 = 1000$ Hz was used. The damping loss factor and modal constant at the second mode shape are considered to be identical to the modal constant and the damping loss factor at the first mode shape. The deduced expression for the ratio σ_1/X_1 in the case of the theoretical system is as follows:

$$\frac{\sigma_1}{X_1}(\omega_1, \eta_1) = \frac{\left|\frac{0.909}{\omega_1^2-\omega^2+\mathrm{i}\eta_1\omega_1^2} + 6.31\cdot 10^{-8} - 1.30\cdot 10^{-10}\ \mathrm{i}\right|}{\left|\frac{0.224}{\omega_1^2-\omega^2+\mathrm{i}\eta_1\omega_1^2} + 1.56\cdot 10^{-8} - 3.20\cdot 10^{-11}\ \mathrm{i}\right|}. \qquad (10)$$

The Eq. (10) is graphically presented in Fig. 4, from which we can conclude that in the case of a phase-locked control loop:

$$\frac{\sigma_1}{X_1} = \text{const.} \qquad (11)$$

holds throughout the whole accelerated fatigue test, although the natural frequency ω_1 and the damping loss factor η_1 change significantly. This observation makes possible the monitoring of the principal stress σ_1 indirectly, using only the measured excitation and response accelerations; however, the ratio σ_1/X_1 must be experimentally obtained before the accelerated fatigue test is conducted. The experimental verification of this theoretical deduction is presented in Section 3.2.

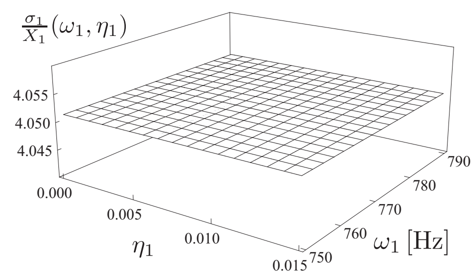

Figure 4: Ratio $\sigma_1/X_1(\omega_1, \eta_1)$ at the changes of ω_1 and η_1.

2.3. Simultaneous identification of natural frequency and damping loss factor.

With the experimental setup and system control, fully explained later in Section 3, it is possible to perform an uninterrupted accelerated fatigue test in the near-resonance area. However, the proposed methodology only controls the reference values of the phase angle ϕ and the principal stress σ_1, and does not account for the identification of the changes of the natural frequency ω_1 and the damping loss factor η_1 during the accelerated fatigue test. Advanced identification methods (e.g. [32]) are not appropriate here and therefore this section presents a simple identification procedure of ω_1 and damping loss factor η_1 in the case of the near-resonant excitation, which is based on the linear SDOF assumption [30]. The linear damping model is assumed for the damping loss-factor identification purposes [16, 33].

In Section 2.2 it was shown that the response of a base-excited structure can be modeled with the modified receptance (Eqs. (6) and (9)):

$$\alpha_{X_a}(\omega) = \frac{\overline{X}_a}{Y} = \frac{{}_pA'_{X_a}}{\omega_p^2 - \omega^2 + \mathrm{i}\eta_p\omega_p^2}, \tag{12}$$

where the SDOF assumption is considered with $B'_{X_a} = 0$. The receptance is fully defined with known values of the natural frequency ω_p, the damping loss factor η_p and the modal constant ${}_pA'_{X_a}$ for the p-th mode shape. These values can be easily determined from the experimentally obtained response of the dynamic system using the circle-fitting method, described in [30].

By measuring the dynamic response of the Y-shaped specimen before the accelerated fatigue test, the initial receptance is obtained with the circle-fitting method. As the accelerated vibration fatigue test starts, the natural frequency ω_1 and the damping loss factor η_1 begin to change, therefore introducing two new variables into Eq. (12) that must be identified. The identification can be made by solving the system of equations:

$$\frac{X_1}{Y} = \left|\alpha_{X_1}(\omega)\right|, \tag{13}$$

$$\phi = \arg(\alpha_{X_1}(\omega)), \tag{14}$$

where the phase angle ϕ, relative response X_1 and excitation Y amplitude are measured during the accelerated fatigue test (Section 3).

3. Experimental procedure

In order to properly excite the specimen in the fourth-mode shape the specimen is fixed as shown in Fig. 1(a). The fixation adapter is attached to the LDS V555 electro-dynamical shaker, which harmonically excites the Y-shaped specimen in the y-axis (Fig. 2) according to Eq (1). By adjusting the excitation amplitude Y and the frequency ω the desired stress load to the specimen can be achieved. However, adjusting the excitation amplitude and frequency is not trivial: as already mentioned, during the accelerated fatigue test the mechanical system of the Y-shaped specimen is changing and real-time control is required. In the following sections we will describe how the excitation frequency ω and the first principal stress σ_1 are controlled.

3.1. Excitation frequency control

During the accelerated fatigue test the natural frequency ω_1 of the specimen decreases as the damage is accumulated in the fatigue zone. In the case of a constant excitation frequency the decrease of the specimen's natural frequency leads to a significant reduction in the response amplitude X_1 and the principal stress σ_1 in the fatigue zone. Furthermore, if the excitation frequency is far from the resonance, the response can have several harmonic components, which complicates the fatigue-life estimation. To keep the system in the resonant area and to prevent the drop in the response amplitude the excitation frequency ω must be tracking the decreasing natural frequency ω_1 in real-time during the accelerated fatigue test.

In the case of a near-resonant single-harmonic excitation of the multi-degree-of-freedom (MDOF) system the tracking of the natural frequency can be performed by maintaining the constant phase shift ϕ between the excitation $y(t)$ and the response displacement $x_1(t)$ (Eqs. (1) and (2), see also Fig. 2 and reference [34]). The constant-phase-shift approach is illustrated in Fig. 5, where two frequency-response-functions (FRFs) of the same Y-shaped specimen are drawn. The response curve with the higher resonance was measured on the intact specimen, and the response curve with the lower resonance was measured after a certain amount of fatigue damage was accumulated by the same specimen. In order to maintain a constant phase shift ($\phi = 175°$ is used in Fig. 5) while the natural frequency ω_1 is decreasing it is necessary to reduce the excitation frequency ω until the reference phase shift ϕ is reached again. Since the excitation $y(t)$ and response $x_1(t)$ are harmonic the phase-shift ϕ measurement is performed in the time domain, as shown in Fig. 2. The feedback loop, based on the phase-shift control, is presented in Fig. 7, *i.e.*, the left loop. In this study the phase shift $\phi = 175°$ was used to avoid the unstable response at, and close to, the phase angle of 90°. Therefore, the system's response becomes stable and easier to control.

The information about the change of the natural frequency ω_1 and the damping loss factor η_1 is important for the *prediction* of the fatigue failure during the service-life [7, 9]. The natural frequency and the damping loss factor identification as discussed in Section 2.3 were used.

3.2. Excitation amplitude control

With the indirect measurement of the principal stress σ_1, described in Section 2.2, it is possible to monitor the stress loading in the fatigue zone. However, it is necessary to define a control method to keep the stress σ_1 within the desired range. Despite the constant phase shift the response-to-excitation ratio $\overline{X}_1/Y$ of the specimen can still vary, mostly due to the increase of the damping loss factor during the fatigue process [9]. The decrease of the ratio $\overline{X}_1/Y$ consequently reduces the stress amplitude σ_1 if the constant excitation amplitude Y is applied. As an example, the relative displacement $X_1(\omega_1, \eta_1)$ during the accelerated fatigue test can be, for a specimen with a close mode at $\omega_2 = 1000$ Hz, written as (6):

$$X_1(\omega_1, \eta_1) = Y\,\omega^2 \left| \cdot \frac{0.224}{\omega_1^2 - \omega^2 + \mathrm{i}\eta_1\omega_1^2} + 1.56 \cdot 10^{-8} - 3.20 \cdot 10^{-11}\,\mathrm{i} \right|. \quad (15)$$

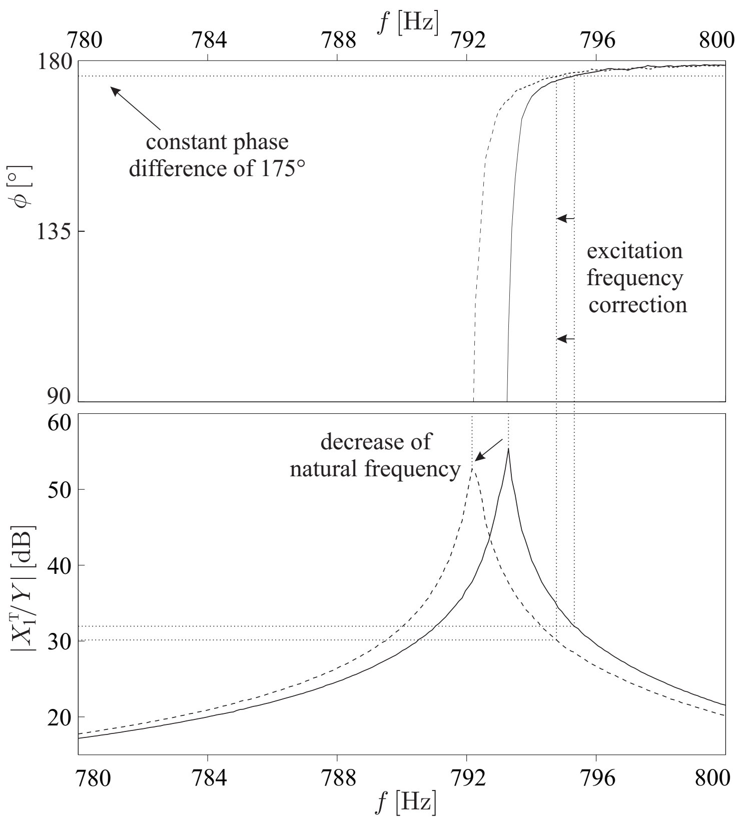

Figure 5: Response of the Y-shaped specimen at the (–) initial state and ($\cdots$) after a certain number of fatigue cycles.

If the excitation amplitude Y is held constant during the accelerated fatigue test, $Y = 1\,\mu$m for instance, the relative displacement reduces when the damping loss factor increases, as shown in Fig. 6.

Based on this observation it is logical to conclude that the excitation amplitude Y must also be controlled in real time during the accelerated fatigue test, to maintain the constant value of X_1 and consequently the constant value of the principal stress σ_1. The appropriate excitation amplitude Y is determined by measuring the difference between the reference value and the measured value of the principal stress σ_1; an increase of the excitation amplitude increases the principal stres. The corresponding control loop is presented in the following Section 3.3.

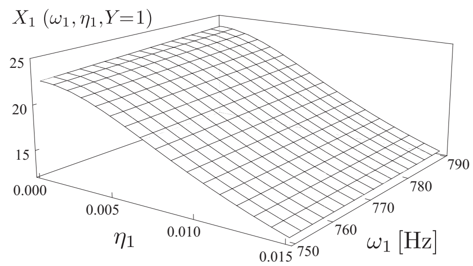

Figure 6: Relative displacement Z during the changes of η_1 and ω_1.

3.3. Control loop

With defined corrections of the excitation frequency ω (Sec. 3.1) and the excitation amplitude Y (Sec. 3.2) the excitation signal is fully defined and generated in real time with the cRIO 9074 controller. The control software was developed in LabView in accordance with the closed feedback control loop shown in Fig. 7. The signals from the accelerometers were acquired with a 24-bit A/D converter, the amplitudes $\overline{X}_1^{\mathrm{T}}$, Y (Eq. (8)) and phase ϕ of the sine signals were determined with the LabView "Tone" module. The values of the instantaneous frequency ω_1 and η_1 were determined according to Eqs. (13) and (14), for the calculation of the σ_{actual} the calibration ratio σ_1/X_1, Eq. (11) was used.

In order to keep the control loop stable, a time of 4 seconds for one control loop was chosen along with the $\pm$ 0.05° and $\pm$ 0.5 MPa of acceptable offset for the phase angle and the stress level, respectively. The values ϕ_{actual} and σ_{actual} are the averaged values for the time of one control loop.

4. Experimental results and discussion

The presented testing methodology was used to conduct an accelerated fatigue test on six specimens: S1, S2, S3, S4, S5 and S6. First, the calibration procedure was performed on the specimens S1, S2 and S3 to confirm the indirect stress measurement methodology, presented in Section 2.2. Second, the accelerated fatigue test was performed on specimens S4 and S5 with excitation in the areas below and above the resonance, respectively; the experiments on the two specimens were repeatedly interrupted to verify the accordance of the identified instantaneous natural frequency (Section 2.3). Finally, to prove the feasibility of the experimental setup and the ad-

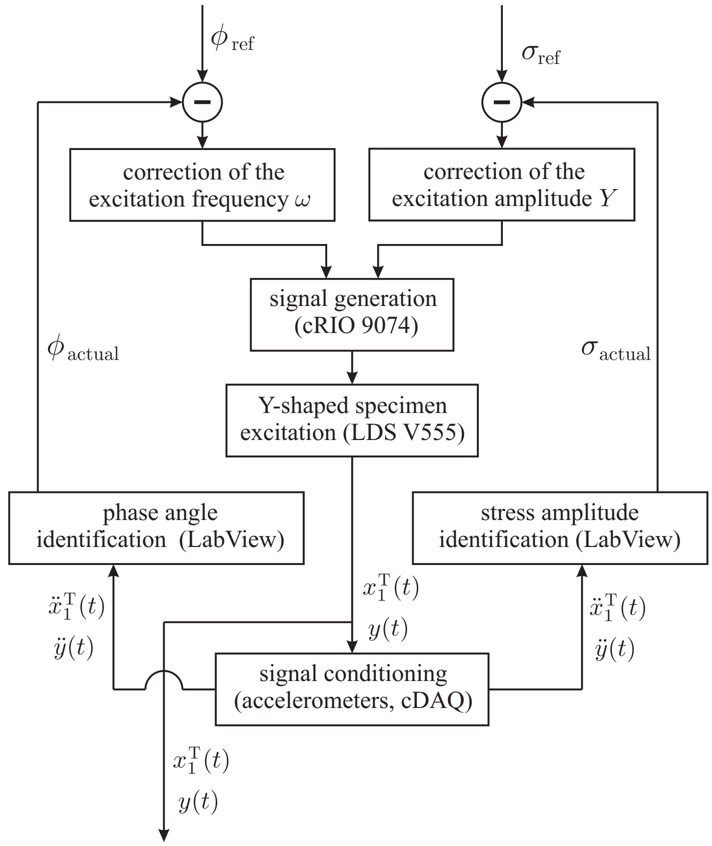

Figure 7: Control loop.

equacy of the presented approach, a continuous accelerated fatigue test was performed on the specimen S6.

4.1. Stress measurement calibration

Before any of the accelerated fatigue tests were conducted, an experimental verification of the indirect stress measurement was performed. The experimental verification was performed in two steps: firstly, the ratio σ_1/X_1 was measured for the three Y-shaped specimens before the accelerated fatigue test and secondly, the σ_1/X_1 ratio was monitored during the accelerated fatigue test of the specimen S3 to confirm the constant value σ_1/X_1 when the modal parameters ω_1 and η_1 begin to change.

Prior to the calibration process the non-uniform stress state in the fatigue zone was analyzed. The stress state in the fatigue zone can be considered as uniform only over the small area at the location of the maximum principal stress σ_1. This implies that a very small strain gauge should be used. However, only a slight mis-location of the small strain gauge could cause moderate measurement errors and issues with the repeatability; therefore, a larger strain gauge was used for the calibration. Because of the nonuniform stress state on the surface, covered by a larger strain gauge, it is necessary to obtain the ratio between the maximum principal stress σ_1 and the average principal stress $\sigma_{1\ \mathrm{average}}$ (the actual value being measured). For the calibration experiment the $\sigma_1/\sigma_{1\ \mathrm{average}}$ ratio was obtained for the strain gauge with a 6-mm measuring grid, Fig. 8 (a). This was done numerically with modal analysis of the finite-element model and experimentally with two strain gauges with measuring grids of 6 mm and 0.6 mm, respectively. The stress measured with the 0.6-mm strain gauge was considered as σ_1. The agreement between the numerical and experimental results was within 1.5% and the ratio of $\sigma_1/\sigma_{1\ \mathrm{average}} = 1.31$ was determined.

Fig. 8(b) shows the relation between the measured principal stress σ_1 and the relative displacement X_1 for the three selected Y-shaped specimens before the accelerated fatigue test was conducted, when no changes of ω_1 and η_1 were present. Fig. 8(b) confirms the linear relation between the principal stress σ_1 and the relative displacement X_1 for the constant natural frequency ω_1 and the damping loss factor η_1. The agreement between the theoretically (Fig. 4) and experimentally (Fig. 8) obtained values for the ratio σ_1/X_1 is very good. The trend-line slopes for the linear regression between the specimens S1-S3 differ by less than 2%, therefore a good repeatability of the indirect stress measurement is confirmed.

Fig. 9 shows the value of the σ_1/X_1 ratio during the accelerated fatigue test of the specimen S3. In this particular experiment the principal stress σ_1 and the relative displacement X_1 were monitored until the failure of the strain gauge occurred after $8 \cdot 10^5$ load cycles (approx. 70% of the specimen's life-time). As predicted by the theoretical analysis in Section 2.2, it can be observed in Fig. 9 that during the experiment the measured ratio σ_1/X_1 remained constant until the strain gauge failure, although the changes in the natural frequency ω_1 and η_1 were present. According to the presented measurements in Figs. 8(b) and 9 the indirect stress measurement offers an accurate monitoring of the principal stress σ_1 during the whole accelerated fatigue test and is not exposed to failure, as in the case of the strain gauge. Additionally, the indirect stress measurement eliminates the measurement

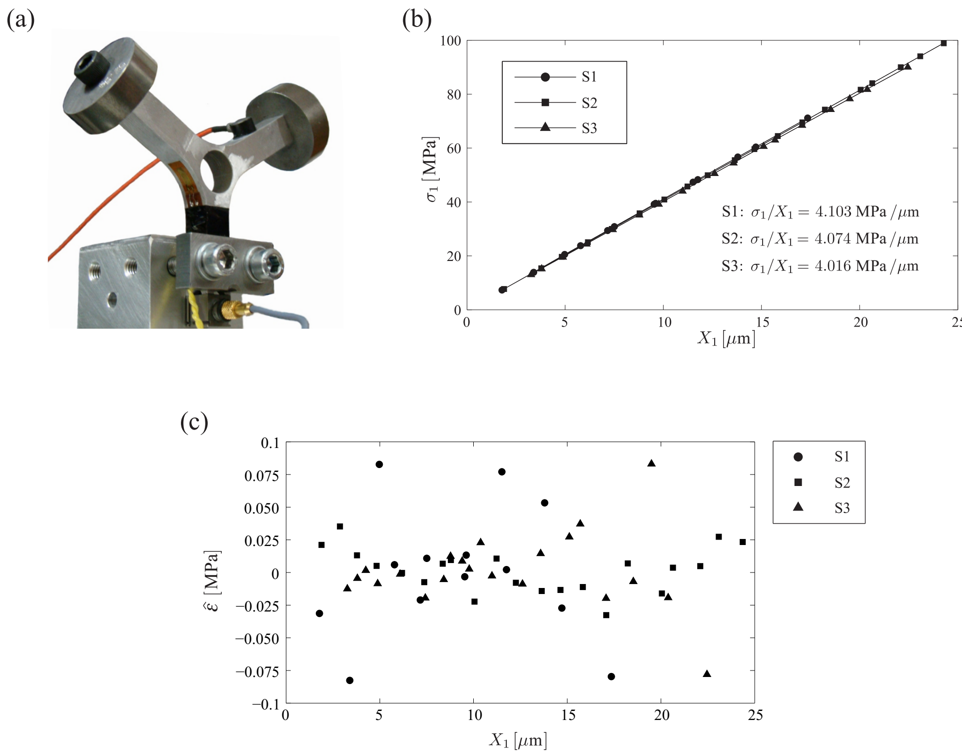

Figure 8: (a) Calibration setup, (b) calibration of specimens S1-S3 and (c) residuals of linear regression.

error due to the inaccurate strain gauge positioning and greatly simplifies the experimental setup and the specimen preparation.

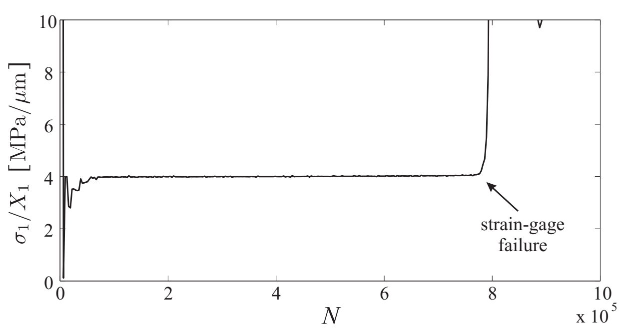

Figure 9: σ_1/X_1 ratio during the accelerated fatigue test of the specimen S3.

4.2. Fatigue test with interruptions

The interrupted accelerated fatigue tests were conducted on the specimens S4 and S5 in order to compare the actual specimen response with the response of a linear SDOF system, as proposed in Section 2.3. The specimens S4 and S5 were excited above and below resonance, respectively; in both cases the reference stress amplitude was set to 125 MPa. The measurement results are shown in Fig. 10, where f denotes the excitation frequency, $f_{1\,\mathrm{harm}}$ denotes the natural frequency, obtained with harmonic excitation, and $f_{1\,\mathrm{rand}}$ denotes the natural frequency, obtained with random broadband excitation. The broadband excitation amplitude was low (root-mean-square value of 3.2 $(\mathrm{m/s^2})^2/\mathrm{Hz}$ in the frequency range from 100 Hz to 1100 Hz) in order to prevent additional fatigue damage to the specimen by broadband excitation.

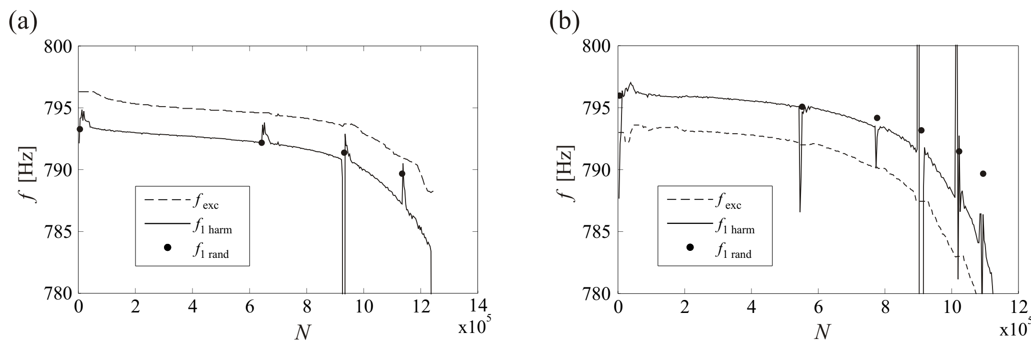

Figure 10: Fatigue test of (a) the specimen S4 and (b) the specimen S5.

From the presented results we can easily observe that the accordance between the instantaneous natural frequencies is very good in the first half of the fatigue process; however, in the second half of the fatigue life significant deviances occur for both specimens, S4 and S5. The interesting observation is that in the case of the excitation below resonance the natural frequency $f_{1\,\mathrm{rand}}$ is receding from the excitation frequency and in the case of the excitation above the resonance the natural frequency $f_{1\,\mathrm{rand}}$ is approaching the excitation frequency, although the phase angle ϕ remains constant in both cases of the accelerated fatigue test. One possible explanation for this behavior is the occurrence of a nonlinearity due to the crack initiation at the middle of the specimen's fatigue life, since the response of a nonlinear system depends on

the type of the excitation (harmonic, broadband) and on the direction of the resonance crossing. To detect the nonlinearity a sine sweep excitation with a reasonably high amplitude could be used; however, a high sine amplitude would cause considerable additional damage to the specimen in the case of resonance crossing, which is not acceptable during the accelerated fatigue test.
Although the identification method with a linear SDOF model does not give exactly the same results as with the broadband excitation, the results can still prove to be useful. When the specimen is excited above the resonance the actual natural frequency remains within the values of the excitation frequency ω and the identified natural frequency ω_1', which is in the case of specimens S4 and S5 is 3 Hz wide or less.

4.3. Fatigue test without interruptions

The final accelerated fatigue test was performed on the specimen S6 above the resonant area a the constant phase angle $\phi = 175°$ and a principal stress amplitude in the fatigue zone of $\sigma_1 = 125$ MPa. The aim of the accelerated fatigue test on the specimen S6 is to verify the realization of the uninterrupted accelerated fatigue test by monitoring the actual principal stress σ_1 and the phase angle ϕ simultaneously with the real-time control of the resonant system near the resonance. The measurements, shown in Figs. 11, 12 and 13, confirm the adequacy of the controller software, since the controlled quantities ϕ and σ_1 remained constant, although the natural frequency of the specimen is reduced by 10 Hz and the damping loss factor increased by almost 100% during the whole fatigue process. Even when the specimen was harmonically excited only 3 Hz from the natural frequency, the whole experiment was stable and well controlled. Additionally, the measurement of the temperature at specimen's fatigue zone showed that the temperature changes due to the structural damping were negligible compared to the changes due to the heat conduction from the shaker (approximately 5°C). However, the temperature increase can present a problem if a material with high internal damping is tested [17].

The final fatigue failure occurred after $1.4 \cdot 10^6$ load cycles, which took only 30 minutes to accomplish. The fatigue crack is shown in Fig. 14 and occurred exactly in the critical fatigue zone, as predicted by the modal analysis.

The specimens S4, S5 and S6 were loaded with a constant stress amplitude of σ_1=125 MPa. The fatigue failures occurred after approx. $1.2 \cdot 10^6$,

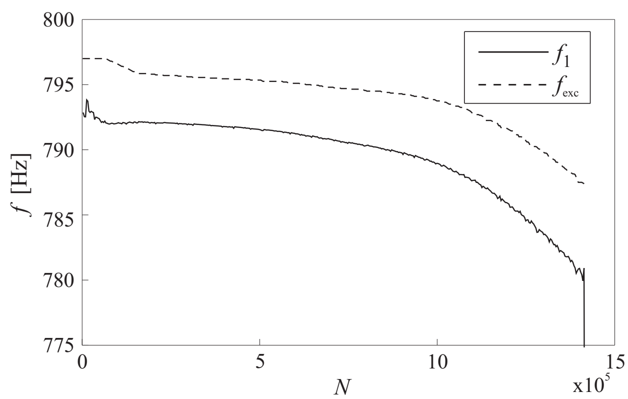

Figure 11: Excitation frequency f and identified natural frequency f_1 during the accelerated fatigue test of specimen S6.

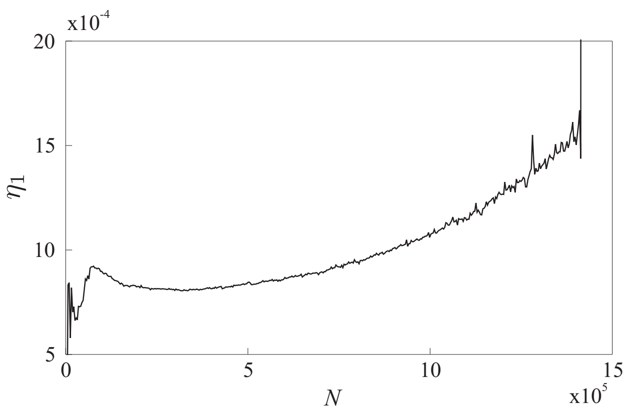

Figure 12: Hysteretic damping loss factor η_1 during the accelerated fatigue test of specimen S6.

$1.1 \cdot 10^6$ and $1.4 \cdot 10^6$ load cycles, respectively. The obtained results show a good repeatability of the fatigue process for the material AS8U3. Similar repeatability was found for stress loads in the range 80–130 MPa.

5. Conclusions

With the presented experimental setup it is possible to perform accelerated fatigue tests using an electro-dynamic shaker. Since the vibrational fatigue approach is proposed, the fatigue zone always appears at a location that is also critical regarding the specimen's dynamic response. Therefore,

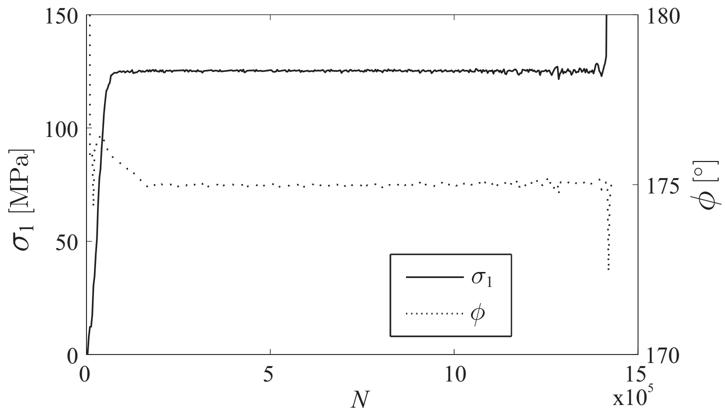

Figure 13: Principal stress amplitude σ_1 and phase angle ϕ during the accelerated fatigue test of specimen S6.

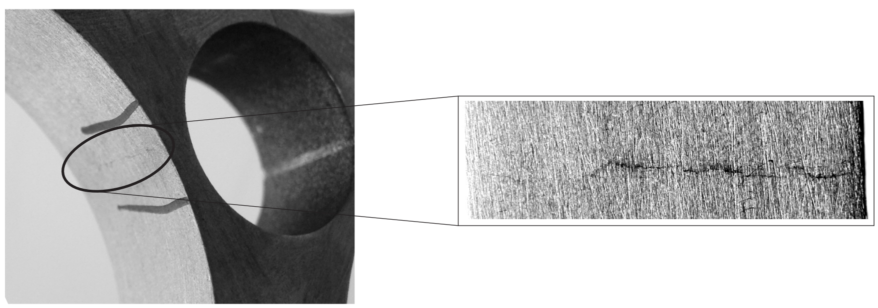

Figure 14: Fatigue crack on the specimen S6.

we can conclude that certain information about the natural frequency change as a function of the accumulated damage will always be obtained. When calculating the vibrational fatigue life of the structure, especially if excited with a narrow-band profile, the frequency change can have a significant influence on the actual fatigue life.

In our research a real-time control of a near-resonant harmonic excitation was developed, based on monitoring the phase angle and the principal stress in a predefined fatigue zone. This approach is applicable to dynamical systems with low damping, which are known to be very unstable when excited near their natural frequency. Besides the issues that arise due to low damping, the presented experimental setup successfully controls the system's stability, even when changes to the natural frequency and the damping loss factor are present. Furthermore, real-time control adequately adjusts the excitation signal to maintain the desired constant value of the stress load during the whole accelerated fatigue test.

The presented experimental approach has several advantages. Firstly, with the described experimental methodology it is possible to perform a fast fatigue test with a simultaneous tracking of the changes of the modal parameters. By exciting the specimen in different mode shapes it is possible to achieve different stress states with a single specimen geometry. Additionally, an indirect measurement of the stress load, based only on measurements of the excitation and response acceleration, greatly shortens the specimen preparation time and additionally improves the reliability of the stress measurement during the whole accelerated fatigue test compared to the traditional strain-gauge method. The developed experimental methodology with certain modifications to the specimen and fixture design can be proposed for the fatigue testing of pre-stressed specimens, different testing temperatures, various stress states, load types (*e.g.*, sine-sweep, random vibrations) and notched specimens.

However, the method itself has some limitations. The first limitation relates to materials with high damping, which causes a reasonable temperature increase during fatigue testing that changes the specimen's modal and material's fatigue properties. The second limitation is the assumption of a linear dynamic system.

In its present state, the experimental setup is used for the rapid acquisition of a material's fatigue parameters, since a high-cycle accelerated fatigue test of $2 \cdot 10^7$ load cycles is achieved in approximately 7 hours. In future work the experimental setup could be used for a validation of vibrational fatigue models.

References

References

[1] D. F. Mazurek, J. T. DeWolf, Experimental study of bridge monitoring technique, Journal of Structural Engineering 116 (1990) 2532–2549.

[2] O. S. Salawu, Detection of structural damage through changes in frequency: a review, Engineering Structures 19 (1997) 718–723.

[3] Y. J. Yan, L. Cheng, Z. Y. Wu, L. H. Yam, Development in vibration-based structural damage detection technique, Mechanical Systems and Signal Processing 21 (2007) 2198–2211.

[4] S. W. Doebling, C. R. Farrar, M. B. Prime, D. W. Shevitz, Damage identification and health monitoring of structural and mechanical systems from changes in their vibration characteristics: a literature review, Technical Report, Los Alamos, New Mexico, 1996.

[5] N. E. Bedewi, D. N. Kung, Effect of fatigue loading on modal properties of composite structures and its utilization for prediction of residual life, Composite Structures 37 (1997) 357–371.

[6] D. G. Shang, M. E. Barkey, Y. Wang, T. C. Lim, Effect of fatigue damage on the dynamic response frequency of spot-welded joints, International Journal of Fatigue 25 (2003) 311–316.

[7] R. J. Wang, D. G. Shang, L. S. Li, C. S. Li, Fatigue damage model based on the natural frequency changes for spot-welded joints, International Journal of Fatigue 30 (2008) 1047–1055.

[8] N. I. Giannoccaro, A. Messina, R. Nobile, F. W. Panella, Fatigue damage evaluation of notched specimens through resonance and anti-resonance data, Engineering Failure Analysis 13 (2006) 340–352.

[9] M. Colakoglu, K. L. Jerina, Material damping in 6061-T6511 aluminium to assess fatigue damage, Fatigue and Fracture of Engineering Materials and Structures 26 (2003) 79–84.

[10] R. O. Curadelli, J. D. Riera, D. Ambrosini, M. G. Amani, Damage detection by means of structural damping identification, Engineering Structures 30 (2008) 3497–3504.

[11] R. J. Wang, D. G. Shang, Fatigue life prediction based on natural frequency changes for spot welds under random loading, International Journal of Fatigue 31 (2009) 361–366.

[12] ASTM, E466 - 07 standard practice for conducting force controlled constant amplitude axial fatigue tests of metallic materials, 2007.

[13] S. R. Swanson, Handbook of fatigue testing, American Society for Testing and Materials, 1974.

[14] S. Vanlanduit, P. Verboven, P. Guillaume, On-line detection of fatigue cracks using an automatic mode tracking technique, Journal of Sound and Vibration 266 (2003) 805–814.

[15] C. Rainieri, G. Fabbrocino, E. Consenza, Near real-time tracking of dynamic properties for standalone structural health monitoring systems, Mechanical Systems and Signal Processing 25 (2011) 3010–3026.

[16] A. L. Audenino, P. M. Calderale, Measurement of non-linear internal damping in metals: processing of decay signals in a uniaxial stress field, Journal of Sound and Vibration 198 (1996) 395–409.

[17] A. L. Audenino, V. Crupi, E. M. Zanetti, Correlation between thermography and internal damping in metals, International Journal of Fatigue 25 (2003) 343–351.

[18] T. J. George, J. Seidt, M. H. H. Shen, T. Nicholas, C. J. Cross, Development of a novel vibration-based fatigue testing methodology, International Journal of Fatigue 26 (2004) 477–486.

[19] T. Nicholas, D. C. Maxwell, Mean stress effects on the high cycle fatigue limit stress in Ti-6Al-4V, Fatigue and Fracture Mechanics 17 (2002) 476–492.

[20] T. J. George, M. H. H. S. O. Scott-Emuakpor, T. Nicholas, C. J. Cross, J. Calcaterra, Goodman diagram via vibration-based fatigue testing, Journal of Engineering Materials and Technology 127 (2005) 58–64.

[21] R. M. French, R. Handy, H. L. Cooper, A comparison of simultaneous and sequential single-axis durability testing, Experimental techniques 30 (2006) 32–37.

[22] L. B. Kheng, K. L. Kean, H. Gitano-Briggs, Design optimisation and fatigue testing of an electronically-driven mechanically-resonant cantilever spring mechanism, Materials and Design 31 (2010) 4023–4028.

[23] N. W. M. Bishop, The use of frequency domain parameters to predict structural fatigue, Ph.D. thesis, University of Warwick, 1988.

[24] Y.-L. Lee, J. Pan, R. B. Hathaway, M. E. Barkey, Fatigue Testing and Analysis (Theory and Practice), Elsevier Butterworth Heinemann, Burlington, Massachusetts, 2005.

[25] M. Boltežar, J. Slavič, Enhancements to the continuous wavelet transform for damping identifications on short signals, Mechanical Systems and Signal Processing 18 (2004) 1065–1076.

[26] A. Preumont, V. Piefort, Prediction random high-cycle fatigue life with finite elements, Journal of Vibration and Acoustics 116 (1994) 245–248.

[27] L. Dietrich, J. Radziejewska, The fatigue damage development in a cast Al-Si-Cu alloy, Materials and Design 32 (2011) 322–329.

[28] R. Gonzalez, D. I. Martinez, J. A. Gonzalez, J. Talamantes, S. Valtierra, R. Colas, Experimental investigation for fatigue strength of a cast aluminium alloy, International Journal of Fatigue 33 (2011) 273–278.

[29] X. Pitoiset, I. Rychlik, A. Preumont, Spectral methods to estimate local multiaxial fatigue failure for structures undergoing random vibrations, Fatigue & Fracture of Engineering Materials & Structures 24 (2001) 715–727.

[30] D. J. Ewins, Modal Testing: Theory and Practice, Research Studies Press Ltd., Letchworth, Hertfordshire, 1984.

[31] A. K. Chopra, Dynamics of Structures: Theory and Applications to Earthquake Engineering, Prentice Hall International, London, third edition, 2007.

[32] J. Slavič, M. Boltežar, Damping identification with the Morlet-wave, Mechanical Systems and Signal Processing 25 (2011) 1632–1645.

[33] H. Liu, J. Wang, Z. Zhang, D. Yuan, L. Liu, Strain-dependent nonlinear damping and application to dynamic analysis of elastic linkage mechanism, Journal of Sound and Vibration 281 (2005) 399–408.

[34] V. Rouillard, M. A. Sek, A frequency domain technique for maintaining resonance condition during sine dwell vibration testing of packages, Packaging Technology and Science 13 (2000) 227–232.

List of Figures